VERIFICATION OF HYDRAULIC PERFORMANCE
OF CONTAINMENT SUMPS
BELLEFONTE NUCLEAR PLANT

by

James B. Nystrom

Prepared for

Tennessee Valley Authority

George E. Hecker, Director

ALDEN RESEARCH LABORATORY
WORCESTER POLYTECHNIC INSTITUTE
HOLDEN, MASSACHUSETTS

May 1982

ABSTRACT

A hydraulic model of the containment building sumps for the Bellefonte Nuclear Plant was constructed at a scale of 1:2.26. Decay heat removal pumps and reactor building spray pumps withdraw water from the sumps after a postulated loss of coolant accident for re-injection into the core and building. To assure acceptable operation of the pumps, the model was tested for a wide range of possible approach flow distributions, grating and coarse screen blockage schemes, and fine screen blockage schemes. The tests were designed to assure that no air entraining vortices were formed, head losses across the screens and in the inlet were acceptable, and swirl in the pump suction pipes was acceptable.

No coherent swirl or vortex activity was noted on the water surface during the testing which included various water levels and prototype velocity tests.

Test results indicated that the maximum swirl angle in the suction inlet was 11 degrees, while average swirl angle was about 3 degrees. Loss measurements indicated an average inlet loss of 0.5 ft, including screen losses for the worst case of 50 percent blockage.

TABLE OF CONTENTS

INTRODUCTION

The reactor containment building of the Bellefonte Nuclear Plant is provided with both a Decay Heat Removal (DHR) system designed to cool the shutdown reactor core and a Reactor Building Spray (RBS) system to cool the containment building, both systems to operate only in the event of a Loss of Coolant Accident (LOCA). Initially, water for these systems is drawn from the borated water storage tank. When the water level in this tank reaches a predetermined level, the decay heat removal system is switched from the injection mode to the recirculation mode. At this point, water is drawn from two containment sumps, which then contain water drained from the break and the containment spray system. Flow approaching the sumps is affected by the geometry of the flow path including various appurtenant structures and equipment. Water level, pump discharge, and water temperature could vary during the recirculation mode, which lasts for an extended period to provide sufficient heat removal.

The Alden Research Laboratory (ARL) of Worcester Polytechnic Institute (WPI) was authorized by the Tennessee Valley Authority to construct and test a model of the Bellefonte Nuclear Plant containment sump with the object of investigating free surface vortex formation, swirl in the inlet piping, inlet losses, or any other flow conditions that could adversely affect the performance of the decay heat removal pumps and the reactor building spray pumps in the recirculation mode. Operating conditions involving a wide range of possible approach flow distributions, grating and coarse screen blockages, fine screen blockages, and combinations thereof were tested in the model.

This report presents the findings of the study and includes a description of the prototype and the model, and summarizes conditions investigated, similitude considerations, test procedures, instrumentation, and interpretation of results.

PROTOTYPE DESCRIPTION

Two reactor building emergency sumps provide redundant drain collection locations which, in the recirculation mode, are sources of water for the Decay Heat Removal and Reactor Building Spray systems after a loss of coolant accident. The emergency sumps are located in the annulus between the secondary shield wall and the primary containment wall with entrances at elevation 622. The secondary shield wall provides protection from missile and water jet impingement after an accident. The Borated Water Storage Tank (BWST) supplies the initial volume of cooling water which is injected into the building while water from the pipe break collects in the reactor building. After a prescribed volume is injected from the BWST, sufficient water is collected to allow the RBS and DHR systems to be switched into the recirculation mode. Figure 1 indicates the location of the sumps within the reactor building and indicates the probable flow paths to the sumps.

Each emergency sump is protected from debris ingestion by a three stage screening system. The first two stages are located on the floor at elevation 622. The coarsest debris is removed by a trashrack having 1 inch by 2 inch bars on 6 inch centers. The rack is 6 ft by 7 ft in plan and is 3 ft high at the lowest point. A 6 inch high curb at the trash-rack prevents settled debris from entering the sump. A 2 mesh screen is located within the trashrack. The screen has a plan area equal to the sump entrance, 4 ft by 5 ft, and is also about 3 ft high at its lowest point. A solid plate covers both the trashrack and the screen. The cover plate has a 5 degree slope to assure that no air will collect. Floor grating 2-1/2 inches deep is attached under the cover plate with bearing bars in the direction of the slope to assist in damping swirl in the approach flow to the sumps. To further suppress circulation of the approach flow which might lead to undersirable vortex action, a pair of floor grating platforms are located above the trashrack and screens. The platforms are 12 ft by 13 ft in plan and are located at elevations 626 ft, 2 inches and 626 ft, 8 inches. The grating is supported by a frame with plan dimensions about equal to the trashrack so that the floor grating, which has a depth of 2-1/2 inches, is cantilevered about 3 ft outside of the trashrack. In some locations, columns, pipes, and walls intrude on the grating platform, reducing its dimensions.

The emergency sump entrance is 4 ft by 5 ft in plan from elevation 622 to elevation 620 after which it expands on one side at a 45 degree angle to 11 ft, 6 inches by 5 ft in plan. Sump B is rectangular in cross-section, while the width of sump A is reduced beginning about halfway along the length to a width of 3 ft, 6 inches. A pair of vertical baffles, which are intended to suppress swirling of the flow, are located in the sump entrance. The baffles extend from elevation 621 ft, 2 inches to 622 ft, 10 inches and form a cross from corner to corner of the sump entrance. The sump descends to elevation 600 and a 1 ft, 6 inch baffle plate across the width of the sump forms basin to collect material which might settle out. A fine screen extends from the top of the baffle to elevation 620. The screen (16 mesh, 0.05 inch openings) is designed to remove debris which could clog the core coolant channels. The screen is sloped 4.5 degrees from vertical toward the direction of flow so that it would tend to be self-cleaning.

A flow guide is installed in the doorway in the secondary shield wall near sump A. Eleven vanes extending from the floor (elevation 622) to elevation 625 are oriented to direct the incoming flow to one side of the sump. A skimmer wall closes the remainder of the doorway. Details of the vortex suppression devices were developed at TVA on a 1:10 scale model (7).

The pump suction lines exit the sumps horizontally 2 ft, 6 inches from the end wall at elevations 603 ft, 5-15/16 inches and 603 ft, 5 inches, for sumps A and B, respectively. The suction line has a 17.25 inch inside diameter, projects 7 1/8 inches into the sump, and has a 3.348 inch radius bellmouth. Floor grating 2-1/2 inches deep is located on two walls and the floor to suppress wall attached vortices. The wall grating extends to elevation 607 ft.

Minimum water level for recirculation mode is elevation 626 ft and maximum is elevation 628 ft. Maximum flowrates for the RHR and RBS pumps are 5,000 gpm and 2,400 gpm, respectively. Makeup water at a flowrate of 800 gpm is also supplied from the sump, resulting in a total maximum flowrate of 8200 gpm per sump.

A site visit was conducted to assure the interpretation and completeness of drawings in regard to the primary approach flow paths, possible secondary approach flow paths, and various equipment obstructing the flow paths.

Various equipment, located below elevation 628 ft, with diameters greater than 3 inches were considered relevant in influencing flow conditions and these are shown in Figure 2. The main pieces of relevant equipment are the reactor coolant drain tank, DHR letdown piping, auxiliary feedwater piping, support columns, and DHR cooler piping. Photographic documentation during the site visit allowed details to be checked as model design and construction proceeded.

SIMILITUDE

The study of dynamically similar fluid motions forms the basis for the design of models and the interpretation of experimental data. The basic concept of dynamic similarity may be stated as the requirement that two systems with geometrically similar boundaries have geometrically similar flow patterns at corresponding instants of time (3). Thus, all individual forces acting on corresponding fluid elements of mass must have the same ratios in the two systems.

The condition required for complete similitude may be developed from Newton's second law of motion:

$$F_i = F_p + F_g + F_v + F_t \qquad (1)$$

where

F_i = inertia force, defined as mass, M, times the acceleration, a

F_p = pressure force connected with or resulting from the motion

F_g = gravitational force

F_v = viscous force

F_t = force due to surface tension

Additional forces may be relevant under special circumstances, such as fluid compression, magnetic or Corriolis forces, but these had no influence on this study and were, therefore, not considered in the following development.

Two systems which are geometrically similar are dynamically similar if both satisfy the dimensionless form of the equation of motion. Equation (1) can be made dimensionless by dividing all the terms by F_i. Rewriting each of the forces of Equation (1) as:

F_p = net pressure x area = $\alpha_1 \Delta p L^2$

F_g = specific weight x volume = $\alpha_2 \gamma L^3$

F_v = shear strees x area = $\alpha_3 \mu \Delta u/\Delta y$ x area = $\alpha_3 \mu u L$

F_t = surface tension x length = $\alpha_4 \sigma L$

F_i = density x volume x acceleration = $\alpha_5 \rho L^3 u^2/L = \alpha_5 \rho u^2 L^2$

where

α_1 α_2, etc. = proportionality factors

L = representative linear dimension

p = net pressure

γ = specific weight

μ = dynamic viscosity

σ = surface tension

ρ = density

u = representative velocity

Substituting the above terms in Equation (1) and making it dimensionless by dividing by the inertial force, F_i, we obtain

$$\frac{\alpha_1}{\alpha_5} E^{-2} + \frac{\alpha_2}{\alpha_5} F^{-2} + \frac{\alpha_3}{\alpha_5} R^{-1} + \frac{\alpha_4}{\alpha_5} W^{-2} = 1 \qquad (2)$$

where

$$E = \frac{u}{\sqrt{\Delta p/\rho}} = \text{Euler number; } \frac{\text{Inertia Force}}{\text{Pressure Force}}$$

$$F = \frac{u}{\sqrt{gL}} = \text{Froude number; } \frac{\text{Inertia Force}}{\text{Gravity Force}}$$

$$R = \frac{u\ L}{\mu/\rho} = \text{Reynolds number; } \frac{\text{Inertia Force}}{\text{Viscous Force}}$$

$$W = \frac{u}{\sqrt{\sigma/\rho L}} = \text{Weber number; } \frac{\text{Inertia Force}}{\text{Surface Tension Force}}$$

Since the proportionality factors, α_i, are the same in model and prototype, complete dynamic similarity is achieved if all the dimensionless groups, E, F, R, and W, have the same values in model and prototype. In practive, this is difficult to achieve. For example, to have the values of F and R the same requires either a 1:1 "model" or a fluid of very low kinematic viscosity in the reduced scale model. Hence, the accepted approach is to select the predominant forces and design the model according to the appropriate dimensionless group. The influence of the other forces would be secondary and are called scale effects (2, 3).

Froude Scaling

Models involving a free surface are constructed and operated using Froude similarity since the flow process is controlled by gravity and inertia forces. The Froude number, representing the ratio of inertia to gravitational force,

$$F = u/\sqrt{gs} \qquad (3)$$

where

u = average velocity in the pipe

g = gravitational acceleration

s = submergence, the representative linear dimension

was, therefore, made equal in model and prototype.

$$F_r = F_m/F_p = 1 \qquad (4)$$

In modeling of an intake sump to study the formation of vortices, it is important to select a reasonably large geometric scale to achieve large Reynolds numbers and to reproduce the curved flow pattern in the vicinity of the intake (4). At sufficiently high Reynolds number, an asymptotic behavior of energy loss coefficients with Reynolds number is usually observed (2). Hence, with $F_r = 1$, the basic Froudian scaling criterion, the Euler numbers, E, will be equal in model and prototype. This implies that flow patterns and loss coefficients are equal in model and prototype at sufficiently high Reynolds numbers. A geometric scale of $L_r = L_m/L_p = 1/2.26$ was chosen for the model, where L refers to length. From Equations (3) and (4), using $s_r = L_r$, the velocity, discharge, and time scales were:

$$u_r = L_r^{0.5} = 1/\sqrt{2.26} = 1/1.50 \qquad (5)$$

$$Q_r = L_r^2\, u_r = L_r^{2.5} = 1/(2.26)^{2.5} = 1/7.70 \qquad (6)$$

$$t_r = L_r^{0.5} = 1/\sqrt{2.26} = 1/1.50 \qquad (7)$$

Similarity of Vortex Motion

Fluid motions involving vortex formation in sumps of low head pump intakes have been studied by several investigators (1, 4, 5, 6).

Viscous and surface tension forces could influence the formation and strength of vortices (1, 5). The relative magnitude of these forces on the fluid inertia force is reflected in the Reynolds and Weber numbers, respectively, which are defined as:

$$R = u\, d/\nu \qquad (8)$$

$$W = \frac{u}{(\sigma/\rho r)^{1/2}} \qquad (9)$$

where r = characteristic radius of vortex and d = intake diameter. It was important for this study to ascertain any deviations in similitude attribitable to viscous and surface tension forces in the interpretation of model results. For large R and W, the effects of viscous and surface tension are minimal, i.e., inertial forces predominate. Surface tension effects are negligible when r is large, which will be true for weak vortices where the free surface is essentially flat. Conversely, only strong air core vortices are subject to surface tension scale effects. Moreover, an investigation using liquids of the same viscosity but different surface tension coefficients ($\sigma = 4.9 \times 10^{3}$ lb/ft to 1.6×10^{3} lb/ft) showed practically no effect of surface tension forces on the vortex flow (1). The vortex severity, S, is therefore mainly a function of the Froude number, but could also be influenced by the Reynolds number.

$$S = S\ (F,\ R) \qquad (10)$$

Anwar (4) has shown by principles of dimensional analysis that the dynamic similarity of fluid motion in an intake is governed by the dimensionless parameters given by

$$\frac{4Q}{u_\theta\, d^2}, \quad \frac{u}{\sqrt{2gs}}, \quad \frac{Q}{\nu\, s}, \text{ and } \frac{d}{2s}$$

where

Q = discharge through the outlet

u_θ = tangential velocity at a radius equal to that of outlet pipe

d = diameter of the outlet pipe

Surface tension effects were neglected in his analysis, being negligible for weak vortices. The influence of viscous effects was defined by the parameter $Q/(\nu\, s)$, known as a radial Reynolds number, R_R.

For similarity between the dimensions of a vortex of strengths up to and including a narrow air-core type, it was shown that the influence of R_R becomes negligible if $Q/(\nu\, s)$ was greater than 3×10^4 (4). As strong air-core type vortices, if present in the model, would have to be eliminated by modified sump design, the main concern for interpretation of prototype performance based on the model performance would be on the similarity of weaker vortices, such as surface dimples and dye-cores. For the prototype of the present study, the values of R_R for the operating temperature ranges of 70° and above, and using the maximum submergence to the entrance of the sump, was greater than 2.75×10^5. In the model, the value of R_R was 6.0×10^4 for Froude scaled velocity for water temperatures of 50°F. Thus, viscous forces would have only a secondary role in the present study. Dynamic similarity is obtained by equalizing the parameters $4Q/u_\theta d^2$, $u/\sqrt{2gs}$, and $d/2s$ in model and prototype. A Froudian model would satisfy this condition.

To compensate for any possible excessive viscous energy dissipation and consequently less intense model vortex, various investigators have proposed increasing the model flow and, therefore, the approach and intake velocity, since the submergence is maintained constant. Operating the model at the prototype inlet velocity (pipe velocity) is believed by some researchers to achieve the desired results (1). This is often referred to as Equal Velocity Rule, and is considered to give conservative predictions of prototype performance. The test procedure for the present study incorporated testing the model at prototype pipe velocities to achieve conservative predictions.

ARL Vortex Activity Projection Technique

ARL has conducted an extensive research program to assure that the conclusions regarding the effect of Reynolds number on vortex activity in the model are valid for the prototype. A technique of extrapolating model vortex activity to prototype Reynolds numbers (17) by using elevated model water temperatures and varying model flow velocity (Froude ratio) has been applied to several studies (12, 17, 18, 19, 29). Figure 3 illustrates the method used to investigate scale effects and predict vortex types in the prototype based on model results (17). The ordinate, F_r, is the ratio of model to prototype Froude number, while the abscissa is the inlet pipe Reynolds number, R. The objective is to determine flow conditions at $F_R = 1$ at prototype R from tests at lower than prototype R. Assume the model to operate at flow less than Froude scaling ($F_r < 1$) at point a_1. By increasing the discharge in the model while keeping the same submergence and temperature, F_r and R are increased corresponding to a point, a_N, where a vortex of type N was first observed. The model Reynolds number can also be changed by varying the kinematic viscosity with temperature changes, and similar tests performed to locate b_N, another point on the locus of type N vortices. Extrapolation of the line of constant vortex strength of type N can be made to a prototype Reynolds number at the proper Froude number (F_r = 1), point P_N. The locus could represent any expedient measure of vortex severity. Any scale effects due to viscous forces would be evaluated and taken into account by such a projection procedure. The high temperature-high flow tests were used in the similar fashion for projecting the inlet loss coefficients (from pressure gradeline measurements) and swirl severities (from vortimeter readings) over a wide range of Reynolds and Froude numbers.

Experience has shown that incoherent swirling flow is even less dependent on Reynolds number than a coherent vortex core. Eliminating the tendency for coherent vortices axiomatically removes possible scale effects. In reactor sumps, the design criteria eliminate the possiblity of coherent vortex cores in an acceptable design.

Figure 4 shows the results of one recirculation sump model (19) which are typical of the other four studies conducted. As can be seen from the data, which are for the final design with vortex suppressor grids, there are no measurable changes in vortex strength with Reynolds number. This is reasonable since the Reynolds numbers are all above the limiting value (1, 4), a previously described similitude requirement. Minor increases in vortex strength occur when the Froude ratio is increased. Other measurements, such as swirl in the inlet pipe, have also shown no measurable dependence on Reynolds number. This indicates that reduced scale model tests are a direct indication of prototype performance for weak vortices, particularly if vortex suppressors are part of the design even at Froude scaled flow (i.e., F_r = 1). Tests at higher than Froude scaled flow are seen to give conservative results, i.e., somewhat stronger vortices than expected in the prototype. Since for this study the minimum Reynolds number is comparable to the minimum for the previous studies which indicated no increase in vortex activity for increasing Reynolds numbers at constant Froude ratio, it is concluded that no scale effects will be present in the final design.

Dynamic Similarity of Flow Through Screens

In addition to providing protection from debris, screens tend to suppress non-uniformities of the approach flow. The aspects of flow through screens of concern in a model study are: (1) energy loss of fluid passing through the screen; (2) modification of velocity profile and the deflection of streamlines at the screen; and (3) production of turbulence. As all these factors could affect vortex formation in a sump with approach flow directed through screens, a proper modeling of screen parameters is important.

The loss of energy across the screen occurs at a rate proportional to the drop in pressure, and this loss dictates the effectiveness of the screen in altering velocity profiles. The pressure drop across the screen is analogous to the drag induced by a row of cylinders in a flow field and could be expressed in terms of a pressure-drop coefficient K (or alternately a drag coefficient), defined as (8),

$$K = \frac{\Delta p}{1/2\ \rho\ U^2} = \frac{\Delta H}{U^2/2g} \tag{11}$$

where

Δp = drop in pressure across the screen
U = mean velocity of approach flow
ρ = density of the fluid
ΔH = head across the screen
g = acceleration due to gravity

From the available literature on the topic (8, 9, 10), it may be seen that

$$K = f(R_s,\ S',\ \text{Pattern}) \tag{12}$$

where

R_s = screen Reynolds number, $U\,d_w/\nu$, d_w being the wire diameter of the screen

S' = solidity ratio, equal to the ratio of closed area to total area of screen

Pattern = geometry of the wire screen

If the solidity ratio and the wire mesh pattern are the same in the model and prototype screens, the corresponding values of K would only be a function of the screen Reynolds number. This is analogous to the coefficient of drag in the case of the circular cylinder. It is known that K becomes practically independent of R_s at values of R_s greater than about 1000 (8,11). However, for models with low approach flow velocity and with fine wire screens, it is necessary to ascertain the influence of R_s on K for both the model and prototype screens before selecting screens for the model which are to scale changes in velocity distribution.

Velocity modification equations relating the upstream velocity profile and downstream velocity profile have been derived based on different theories (8). Most of these indicate a linear relationship between upstream velocity, profile, and downstream velocity profile, shape and solidity ratio of screen, and value of K. If the wire shape and solidity ratios are the same in the model and prototype screens, it is possible to select a suitable wire diameter to keep the values of K approximately the same for the model and prototype screens at the corresponding Reynolds number ranges. Identical velocity modifications would be produced by the respective screens if the loss coefficients were identical.

The pressure loss coefficient to Reynolds number relationship of fine screens have been investigated at ARL (12). Based on the similarity of pressure loss and velocity modifications, the prototype screen was chosen. Since the model screen Reynolds number would be about 45% that of the prototype for Froude scale velocity, this was considered sufficiently high to simulate losses adequately and, therefore, velocity profile modifications. In any case, screen blockages cause changes in velocity distributions far outweighing changes due to screen.

MODEL DESCRIPTION

The model was constructed to a geometric scale of 1:2.26 with boundaries, as indicated in Figure 5. Model boundaries were chosen at locations where flow pattern control in the prototype would be sufficiently removed from the sumps to avoid boundary effects, especially once screen blockage is considered. Screen blockage has consistently generated the most severe vortices and swirl in the numerous past ECCS sump studies at ARL. The model was located in an existing elevated tank to provide sufficient room to install the sumps and to allow access to observe flow patterns in the sumps. Figures 6 through 8 show the completed model from various perspectives.

A centrifugal pump recirculated water from the sumps into the model inlets. Water level in the model was controlled by addition of water from an existing sump. Valves in the supply lines and an elbow meter in one supply line allowed the distribution of flow to the major flow entrances to be varied. Flow straighteners and screens at the model boundaries provided a uniform initial velocity distribution with relatively low turbulence levels and removed any debris which might clog the sump screens. Portions of the prototype structure with outside dimensions greater than 3 inches, such as pipes, columns, pipe supports, and the RC drain tank, in the immediate vicinity of the sump and below the water surface were modeled to the geometric scale, as shown in Figure 2.

The model was constructed basically of wood, with steel sumps having clear acrylic windows which allowed observation of flow patterns. The suction pipe of sump B was modeled for about 40 pipe diameters, had an access port for vortimeter installation, and had 12 sets of piezometers for pressure gradeline measurement. ASME standard orifice flowmeters were provided to measure flow in each suction line.

The floor grating platforms, trashracks, and coarse screens are shown in Figures 6 and 7 for sumps A and B. Piping details included in the model are shown in Figure 8 looking from sump B in the direction of sump A. Clear PMMA plastic was used for sump covers to allow observation of flow patterns between the screens. A flexible membrane was installed on a roller device to allow coarse screen blockages to be changed without model disassembly. Fine screen blockages were mounted on hinges with actuating rods extending above the water surface to allow rapid changes of blockage configuration. Model screens were the same as the prototype screens. The coarse screen was 2 inch mesh with 0.080 inch wire diameter, and the fine screens were 16 inch mesh with 0.010 inch wire diameter. In critical areas, such as the platforms and under the cover plates, the floor grating used in the model was prototype dimensions. In the sump, the depth of the grating was scaled using standard floor grating having fewer, thicker bearing bars.

INSTRUMENTATION AND OBSERVATION TECHNIQUES

Flow Measurement

Flowrates were measured by ASME standard orifice meters and coefficients using air-water manometers for differential pressure measurement.

Pressure Gradelines

The pressure gradeline in the suction line for sump B was measured by pairs of piezometers at 12 locations using air-water manometers with the sump water level as reference pressure. The pressure gradeline was extrapolated to the entrance by a linear least squares curve fit of the pressure measurements. The area average velocity was used to calculate the pipe velocity head, which was added to the extrapolated pressure gradeline. The pipe total head was subtracted from the sump total head to determine the inlet loss. An entrance loss coefficient was calculated by:

$$K = \frac{\Delta H_i}{\frac{U^2}{2g}} \qquad (13)$$

where

K = loss coefficient

ΔH_i = inlet head loss, ft

Pipe Swirl

Average swirl in the suction pipes was measured by cross vane swirl meter. Studies at ARL (22) have shown that a swirl meter with vane diameter 75% that of the pipe diameter best approximates the solid body rotation of the flow. The rate of rotation of the vortimeter was determined by counting the number of blades passing a fixed point in two minutes.

An average swirl angle was defined as the arctangent of the maximum tangential velocity divided by the axial velocity. The maximum tangential velocity is the rotational speed times the circumference of the pipe, π d N, and the average swirl angle is defined by:

$$\theta = \arctan\left(\frac{\pi \; d \; N}{U}\right) \tag{14}$$

where

N = revolutions per second

d = pipe diameter, ft

U = mean axial velocity, ft/sec

Vortex Activity

Vortex activity was recorded by observing vortex strength on a scale from 1 to 6 (see Figure 9). Vortex strength was identified by using dye injection or addition of "trash" consisting of a slightly buoyant ball of paper when required.

Observation of Flow Patterns

Visual aids, such as dye, were used to observe flow patterns. Photographic documentation was taken whenever appropriate.

TEST PROCEDURE

Tests were conducted at the normal laboratory water temperature. The model was filled to an appropriate level, and all piezometer and manometer lines were purged of air and zero flow differentials checked. The required flowrates were then set and allowed to stabilize. The water level was checked and adjustments made if required and flowrates were rechecked and re-adjusted, if necessary. A 15 minute minimum settling time was allowed prior to initiation of the data recording. Fifteen minutes of vortex observations were recorded and the required physical parameters, such as depth, manometer deflections, and swirl meter readings, were recorded. Entrance losses were determined with swirl meters removed for selected conditions.

TEST RESULTS

The six blockages of the coarse screen and grating shown in Figure 10 were tested. For convenience, these were called upper blockages. The fine screen in the sump was blocked with the fourteen geometries shown in Figure 11.

The majority of the testing was conducted with equal approach velocity distribution, 4 ft water depth, and Froude scale velocity. For the above conditions, three upper blockages, 3, 4, and 5, were tested with all the fine screen blockages and three upper blockages, 1, 2, and 3, were tested with fine screen blockage cases 2, 5, 8, 13, and 14. No coherent surface swirl or vortex activity was noted for any of the above tests. The maximum surface disturbances were transient swirls which were caused by the shear layers due to the relatively high velocity flow from the two doorways which supplied the flow and these swirls were well separated from the sumps.

Since surface activity would not be affected by the fine screen blockage geometry located deep within the sump, the upper blockage geometries were tested for several variations of approach distribution, water depth, and velocity scale for a single fine screen blockage. The extreme approach distributions of the entire flow from either side was tested for each upper blockage geometry at Froude scale velocity. Surface activity near the sump located away from the inlet flow was decreased since the approach velocities were decreased from the equal approach distribution case. The surface activity of near the other sump was increased due to the increased inlet velocity, but in no case were any coherent vortices or swirl noted.

The effect of water level was demonstrated by slowly changing the water level and observing the surface activity. This was accomplished for three upper blockage geometries, 2, 5, and 6 with the equal and the two extreme approach flow distributions and prototype velocity. No significant changes of surface activity were noted as the depth was changed. The decrease in approach velocity as the depth increased, decreased the turbulence levels and apparent surface activity. The change to prototype velocity increased the surface activity, but no coherent swirl or vortex activity was noted.

Various changes in the flow path were made to determine if an effect on surface activity was possible. The addition of small disturbances on the secondary shield wall to simulate increased roughness due to small equipment such as electrical boxes or conduit, did not produce a significant effect on either the flow patterns or surface activity. The entrance flow distribution at sump B was modified by changing the balance of the flow from the two straighteners and, while the initial flow patterns were modified, the surface activity near the sump was unchanged. The flows from the three drain lines in the secondary shield wall were interrupted with no observable change to the surface activity near the sumps.

An intermittent submerged vortex was noted in four tests. Fine screen blockage #4 produced a submerged vortex which entered the suction pipe in sump A for Froude scale velocity for both uniform approach flow and the condition in which all flow entered near sump A. The vortex was noted only for upper blockage #4. With prototype velocity scale, fine screen blockage #8 caused a submerged vortex with upper blockage #1 in sump B and with upper blockage #3 in sump A. These vortices were transient and existed for less than about 25% of the time. The swirl angle measured in these cases was greater than 5 degrees, but was not the maximum value determined.

In no case tested was surface coherent swirl or vortex activity noted.

SWIRL ANGLE

Swirl angle was determined as a two minute (model time) average value. Table 1 lists measured swirl angles for Froude scale velocity with 4 ft water depth and equal approach flow distrubution for various combinations of coarse screen and grating blockage and fine screen blockage. The maximum swirl angle determined was 11.1 degrees for sump A with upper blockage #2 and fine screen blockage #4. The average swirl angle for all blockages tested was 3.3 degrees for sump A. Fine screen blockage #4 resulted in the greatest swirl angles, averaging greater than 8 degrees for the four upper blockages tested. Blockage #8 was the only other case where the average of the swirl angles was greater than 5 degrees. Swirl angles measured for sump B were generally less than those in sump A and the average for all tests was 2.9 degrees. The decrease in swirl angle was probably due to the lower approach velocity in sump B, since sump A had a decreasing width after the fine screen. Fewer swirl measurements were conducted for sump B since the swirl meter was removed for some tests to allow determination of the inlet losses. For sump B, the maximum swirl angle measured was 9.7 degrees for upper blockage #1 and fine screen blockage #14. Fine screen blockage #14 resulted in the highest swirl angles for sump B.

The effect of the approach flow distribution is shown in Table 2. For clean screens, the variation of the approach flow distribution caused significant variation in swirl angle, but when fine screen blockages were used, the variation due to the approach flow distribution was small. A maximum increase of 2 degrees was noted, while decreases of greater than 2 degrees were noted from the base case of equal flow distribution. The fine screen blockage cases with the maximum swirl angles were specifically chosen to demonstrate the effect of approach flow distribution for various upper blockages. Swirl angle was not constant with time, and repeat measurements indicated variations of

TABLE 1

Swirl Angle

Sump A

Fine Screen Blockage	Upper Blockage 0	1	2	3	4	5	6
0	0.6	0.7	1.0	0.4	1.8	-2.0	3.7
1					-1.8	-5.2	-4.2
2		-2.3	0.6	-0.6	0.7	-5.3	2.3
3					5.3	0.7	8.0
4			11.1		8.6	5.7	7.6
5		1.4	2.4	2.7	5.3	-5.2	2.0
6					2.7	-0.6	3.6
7					-3.2	-5.2	-2.5
8		-6.8	-6.0	-7.5	-4.2	3.7	-5.6
9					3.8	-1.9	2.4
10					1.3	-3.8	-2.2
11					0.6	-2.7	2.8
12					0.4	-3.9	0.4
13		-1.1	-0.4	-2.2	-1.0	-6.0	-2.7
14		2.6	2.5	3.4	5.1	3.3	8.2

NOTE: Equal approach flow distribution: 4 ft depth: Froude velocity scale

Table 1 (Con't)

Sump B

Fine Screen Blockage	Upper Blockage 0	1	2	3	4	5	6
0	0.5	1.0	0.1			0.3	3.9
1						-3.9	-1.8
2		-3.1	0.1			-3.4	1.0
3						-2.0	6.3
4						2.5	5.1
5		5.5	6.0			-5.1	6.5
6						3.4	7.7
7						-3.3	4.6
8		-6.2	-7.2			-6.8	-6.0
9						1.8	5.7
10						0.3	-0.9
11						-0.3	3.4
12						2.2	5.5
13		-0.6	-2.0			-1.9	0.8
14		9.7	5.6			6.0	8.3

TABLE 2

Effect of Approach Flow Distribution on Swirl Angle

Blockages		Sump A			Sump B		
Upper	Fine	50-50	100-0	0-100	50-50	100-0	0-100
-	-	0.6	5.0	-0.4	0.5	2.3	0.6
5	-	-2.0	-0.8	1.1	0.3	0.3	-0.8
2	8	-6.0	-6.1	-5.6	-7.2	-6.3	-6.8
1	8	-6.8	-6.6	-4.6	-6.2	-2.8	-8.2
3	8	-7.5	-8.3	-3.4			
4	4	8.6	9.3	8.5			
6	14	8.2	9.2	4.6	8.3	6.1	7.3
2	2	1.7	1.9	-0.8	-2.5	-0.6	-2.0

about 1 degree could be expected due to the unsteady nature of the swirl. Therefore, the variations with approach flow distribution are not significant. Also, the fine screen blockage controls the swirl angle as can be noted by the nearly constant swirl angle measured for three different upper blockage cases with fine screen blockage #8.

Tests with prototype scale velocity and greater water depths showed no significant variation in swirl angle, as would be expected. Since the suction inlet has a straight run of about 19 pipe diameters prior to a pair of 90 degree flows, the swirl angle measured near the inlet will decay considerably. Using a conservative estimate for the swirl decay parameter, beta = 0.02, from available literature (27, 28), the swirl remaining at the end of the straight pipe will be about 68 percent of the original swirl. This results in a maximum swirl angle of about 7.5 degrees and an average swirl angle of slightly greater than 2 degrees. Swirl angles of similar magnitudes may result from combined bends (25, 26). Therefore, the measured swirl angles are not considered excessive.

INLET HEAD LOSSES

Inlet losses were measured and an inlet loss coefficient calculated by equation (13). The measured inlet loss includes the losses due to the screens and grating. Losses were measured for four upper blockages and for upper blockage #4, all fine screen blockages were used. Table 3 lists the head loss in ft prototype and the inlet loss coefficient. The average loss coefficient for upper blockage #4 was 0.49 ft corresponding to a loss coefficient of 0.25. The maximum loss measured was for no fine screen blockage and equalled 0.53 ft. The minimum loss was 0.45 ft for fine screen blockage 11. The range of ± 0.04 ft is due to the measurement accuracy and an uncertainty of that order is to be expected. The loss for upper blockage 3 averaged 0.43 ft and upper blockage #5 resulted in a loss of 0.49 ft. The maximum loss measured was 0.65 ft for upper blockage #2 with fine screen blockage #4.

The measured loss coefficients are somewhat higher than those predicted for a bellmouth inlet, but this would be expected since screen and sump entrance losses are included. The accuracy of the loss measurements is limited by the flowmeter accuracy. Since ASME standards were used for construction and for the coefficient, an accuracy of about $\pm$ 5% would be expected. The magnitude of the losses is small and errors even larger than 5% would have a minimal impact on the overall calculations of losses to the pumps.

TABLE 3

Inlet Losses

Blockages Upper	Blockages Fine	Head Loss Feet	Loss Coefficient
4	-	0.53	0.26
4	1	0.48	0.24
4	2	0.50	0.25
4	3	0.49	0.25
4	4	0.49	0.25
4	5	0.48	0.24
4	6	0.47	0.24
4	7	0.50	0.25
4	8	0.47	0.24
4	9	0.49	0.25
4	10	0.52	0.26
4	11	0.45	0.23
4	12	0.50	0.25
4	13	0.51	0.26
4	14	0.48	0.24
3	-	0.41	0.21
3	5	0.45	0.23
3	8	0.43	0.22
2	5	0.60	0.31
2	4	0.65	0.33
2	8	0.61	0.31
2	13	0.61	0.31
2	14	0.61	0.31
5	13	0.49	0.25

SUMMARY

A 1:2.26 scale model of the containment building sumps for the Bellefonte Nuclear Plant were constructed and tested. In the recirculation mode, decay heat removal and reactor building spray withdraw water from two containment sumps after a postulated loss of coolant accident. A coarse trashrack and 2 mesh vertical screen surround each pump sump and a fine screen within the sumps assure no debris is entrained into the pumping systems. Debris could block trashrack, coarse screen, and fine screen, thereby producing adverse flow patterns in the sump. A wide range of possible approach flow distributions, trashrack and coarse screen blockages, fine screen blockages, and combinations thereof were tested to simulate possible undesirable flow patterns which could result in poor pump performance during the recirculation mode. The model was operated with both Froude scale velocity and prototype velocity. Vortex activity was observed and recorded. Head losses due to the trashrack with a range of water levels, screens, and pump inlet and the flow rotation in the suction pipe were also measured.

No surface vortex activity was observed during any of the tests. Average swirl angle in the suction pipes was less than 4 degrees and maximum value measured was 11.1 degrees. Inlet losses varied from about 0.41 ft to 0.65 ft for the worst case of 50 percent screen blockage. The pipe inlet head loss averaged less than 0.3 times the inlet pipe velocity head.

REFERENCES

1. Daggett, L.L., and Keulegan, G.H., "Similitude Conditions in Free Surface Vortex Formations," Journal of Hydraulics Division, ASCE, Vol. 100, pp. 1565-1581, November 1974.

2. Daily, J.W., and Harleman, D.R.F., Fluid Dynamics, Addison-Wesley Publishing Company, 1965.

3. Rouse, H., Handbook of Hydraulics, John Wiley & Sons, 1950.

4. Anwar, H.O., Weller, J.A., and Amphlet, M.B., "Similarity of Free-Vortex at Horizontal Intake," Journal of Hydraulic Research, IAHR 16, No. 2, 1978.

5. Hattersley, R.T., "Hydraulic Design of Pump Intakes," Journal of the Hydraulics Division, ASCE, pp. 233-249, March 1965.

6. Reddy, Y.R., and Pickford, J., "Vortex Suppression in Stilling Pond Overflow," Journal of Hydraulics Division, ASCE, pp. 1685-1697, November 1974.

7. Harshbarger, E.D., "Bellefonte Nuclear Plant Model Tests 1:10 Scale DHR Sumps," Report No. WR28-1-88-101, Tennessee Valley Authority, September 1979.

8. Baines, W.D., and Peterson, E.G., "An Investigation of Flow Through Screens," Trans. ASME, pp. 467-477, July 1951.

9. Papworth, M., "The Effect of Screens on Flow Characteristics," British Hydromechanics Research Association, Report TN1198, November 1972.

10. Weighardt, K.E.G., "On the Resistance of Screens," The Aeronautical Quarterly, Vol. IV, February 1953.

11. Tennessee Valley Authority, "Flow Through Screens," Report No. 87-8, May 1976.

12. Padmanabhan, M., "Hydraulic Model Studies of the Reactor Containment Building Sump, North Anna Nuclear Power Station - Unit 1," ARL Report No. 123-77/M250CF, July 1977.

13. Govier, G.W., and Aziz, K., "The Flow of Complex Mixtures in Pipes," Van Nostrand Reinhold, 1972.

14. Chainshvili, A.G., "Air Entrainment and Vertical Downward Motion of Aerated Flows," IAHR, 8th Congress, Montreal, Canada.

15. Muakami, M., Suehiro, H., Isaji, T., and Kajita, J., "Flow Entrained Air in Centrifugal Pumps," 13th Congress, IAHR, Japan, August 31 - September 5, 1969.

16. Final Safety Analysis Report, J.M. Farley Nuclear Plant, Appendix 60, Nuclear Regulatory Commission, 1977.

17. Durgin, W.W., and Hecker, G.E., "The Modeling of Vortices at Intake Structures," Joint Symposium of Design and Operation of Fluid Machinery, Colorado State University, June 1978.

18. Padmanabhan, M., "Hydraulic Model Investigation of Vortexing and Swirl Within a Reactor Containment Recirculation Sump," Donald C. Cook Nuclear Power Station, ARL Report No. 108-78/M178FF.

19. Padmanabhan, M., "Assessment of Flow Characteristics Within a Reactor Containment Recirculation Sump Using a Scale Model," McGuire Nuclear Power Station, ARL Report No. 29-78/M208JF.

20. Padmanabhan, M., "Selection and Scaling of Horizontal Gratings for Vortex Suppression," ARL Report No. 68-78, July 1978.

21. Padmanabhan, M., and Vigander, S., "Pressure Drop Due to Flow Through Fine Mesh Screens," Journal of the Hydraulics Division, ASCE, HY8, August 1978.

22. Durgin, W.W., and Lee, H.L., "The Performance of Cross-Vane Swirl Meters," ASME Winter Annual Meeting, 1980.

23. Miller, D.S., Internal Flow Systems, BHRA Fluid Engineering, 1978.

24. Unpublished ARL Experimental Results.

25. Padmanabhan, M., "Investigation of Flow Distribution and Swirl Due to a Combined Pipe Bend," McGuire Nuclear Power Station, ARL Report No. 12-79/M208MF, December 1978.

26. Nystrom, J.B., "The Effects of Combined Bends on the Velocity Distribution and Swirl at the Inlet to a Pump," ARL Report No. 122-80/M105AF, August 1980.

27. Baker, D.W., and Sayre, C.L., "Decay of Swirling Turbulent Flow of Incompressible Fluids in Long Pipes," Flow, Its Measurement and Control in Science and Industry, 1974.

28. Janik, C.R., and Padmanabhan, M., "The Effect of Swirling Flow on Pipe Friction Losses," ARL Report No. 26-81/M296KF, February 1981.

29. Padmanabhan, M., "Investigation of Vortexing and Swirl Within a Containment Recirculation Sump Using a Hydraulic Model," ARL Report No. 25-81/M296HF, February 1981.

FIGURES

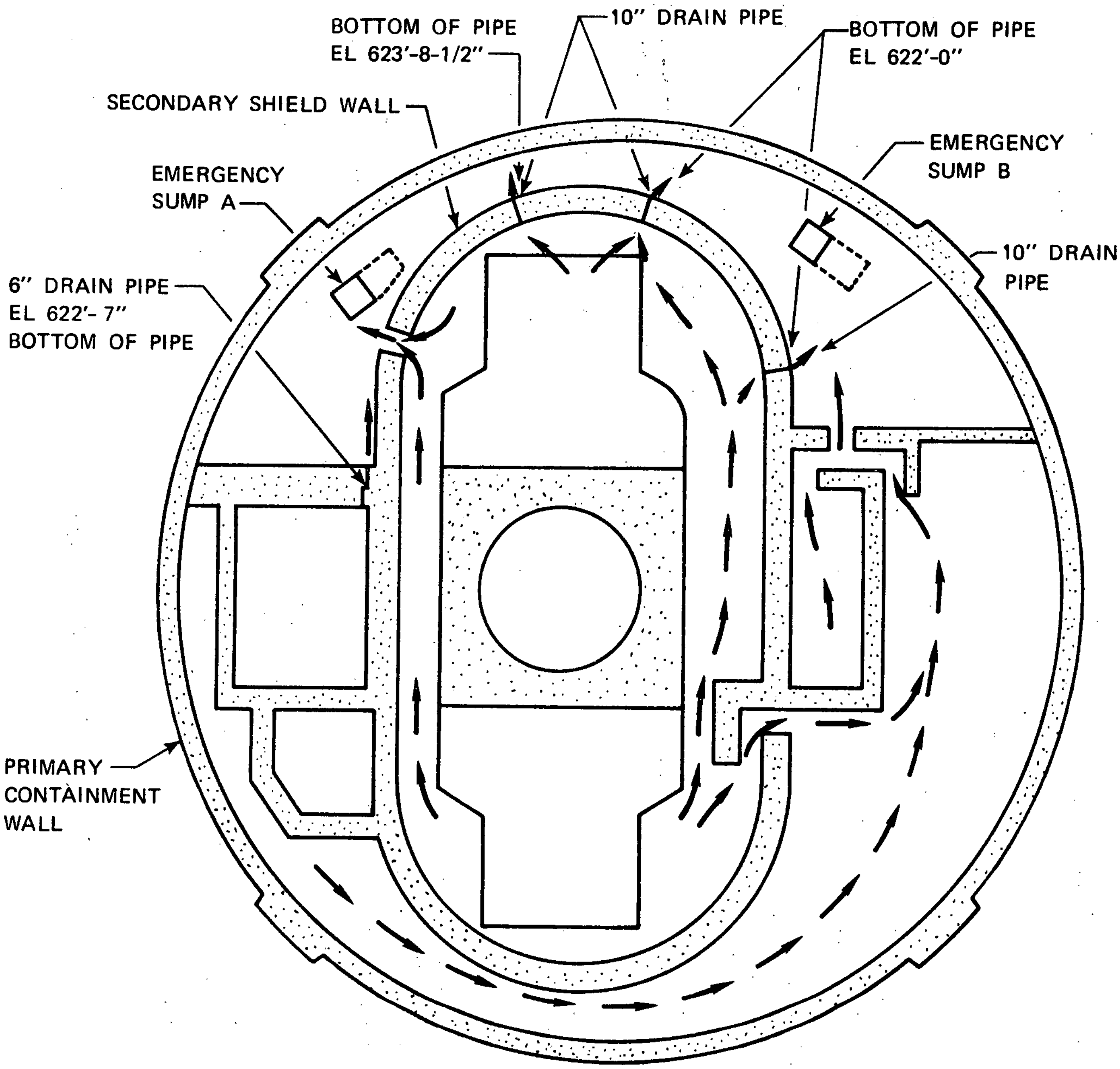

FIGURE 1 PLAN OF REACTOR CONTAINMENT BUILDING AT ELEVATION 622 SHOWING FLOW PATHS TO EMERGENCY SUMPS

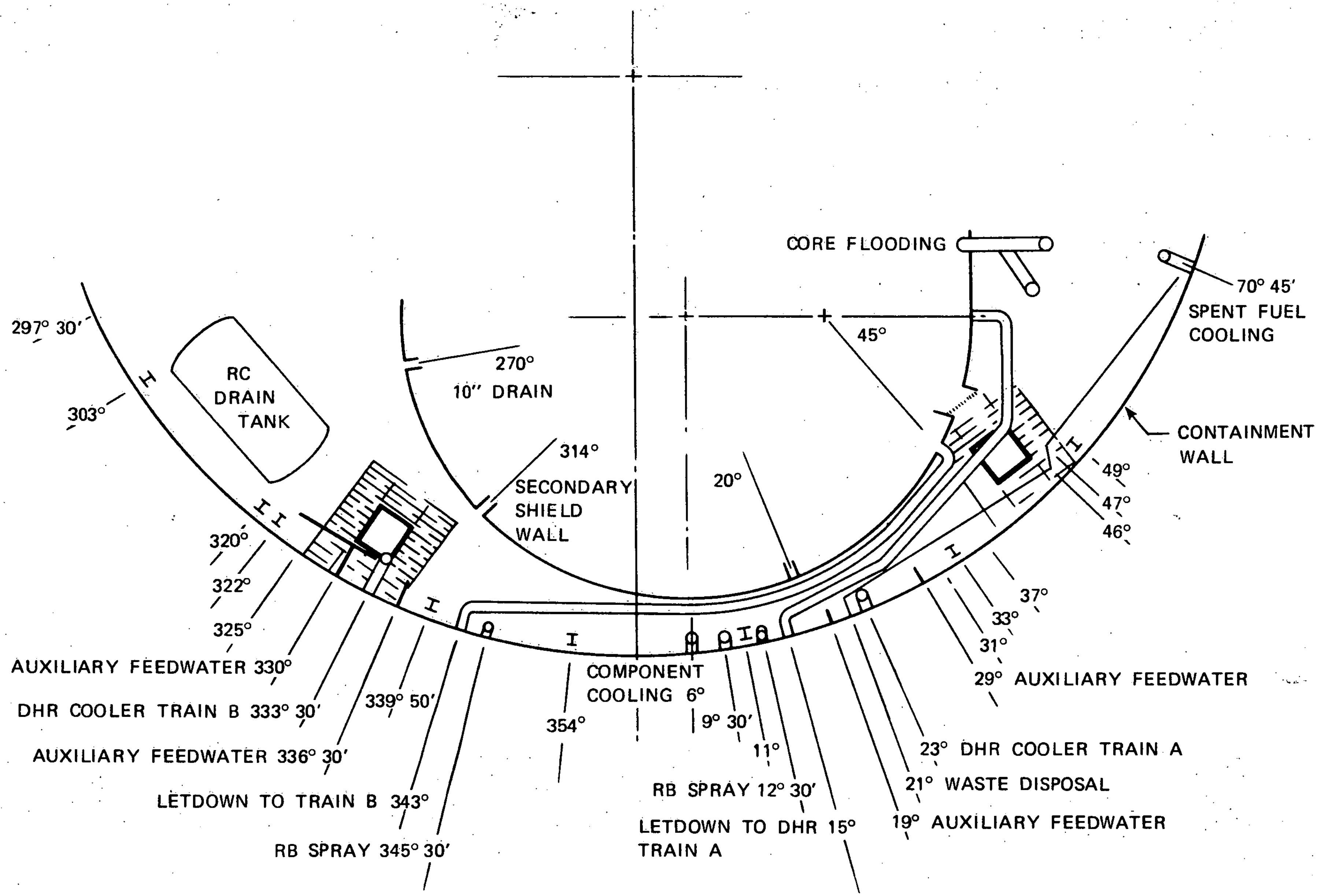

FIGURE 2 EQUIPMENT NEAR SUMPS

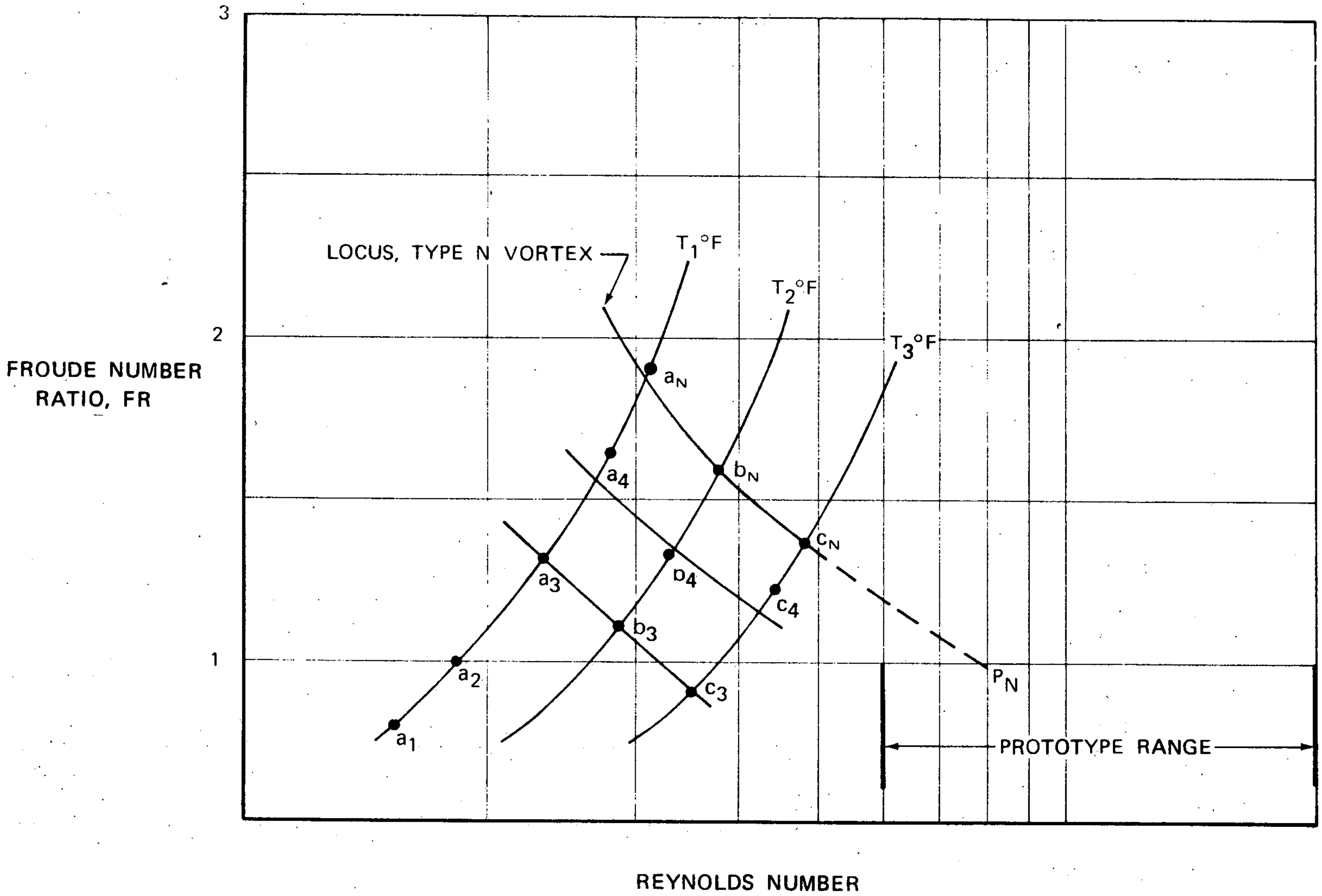

FIGURE 3 ARL VORTEX ACTIVITY EXTRAPOLATION TECHNIQUE

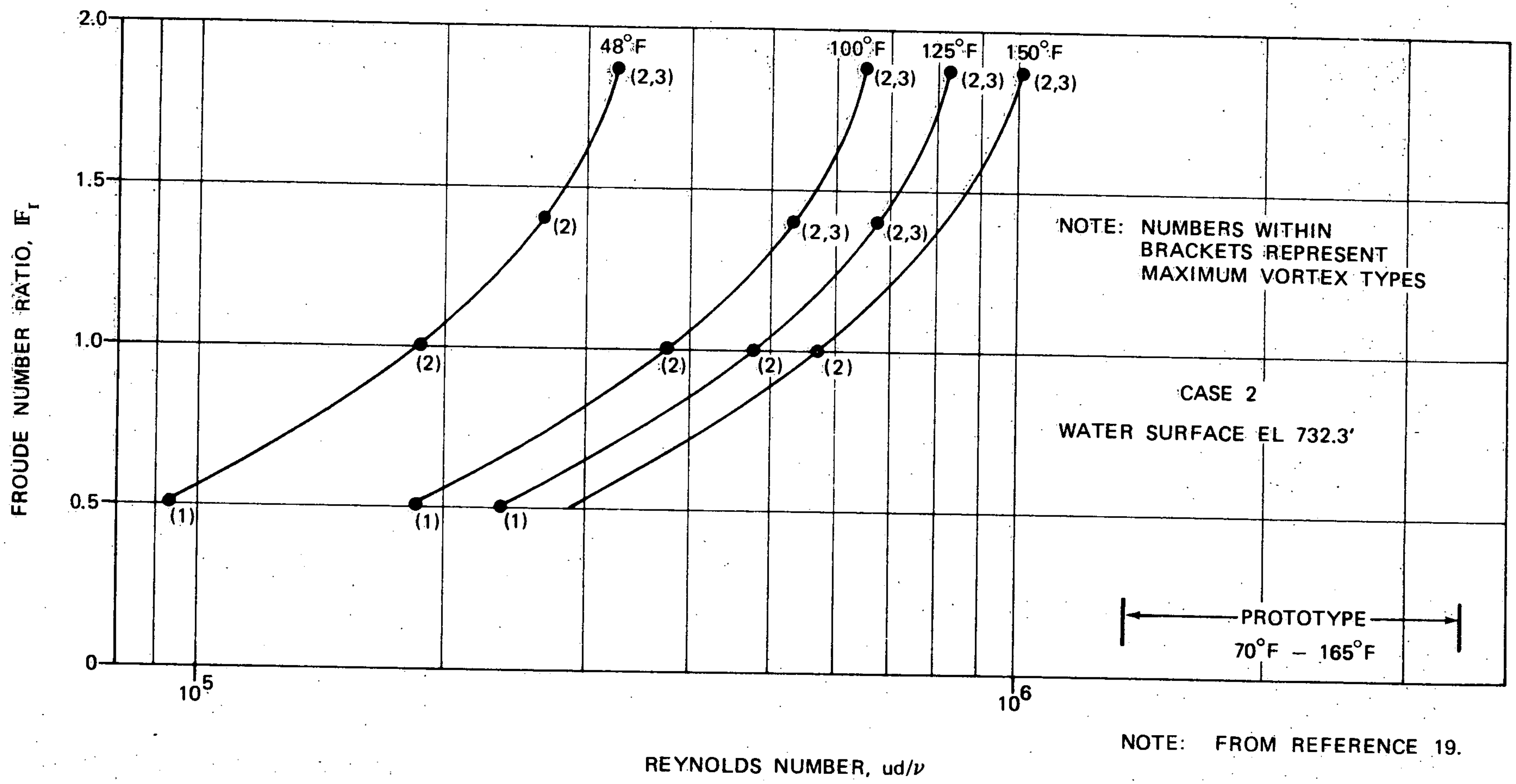

NOTE: FROM REFERENCE 19.

FIGURE 4 TYPICAL MODEL RESULTS FOR ARL VORTEX EXTRAPOLATION TECHNIQUE

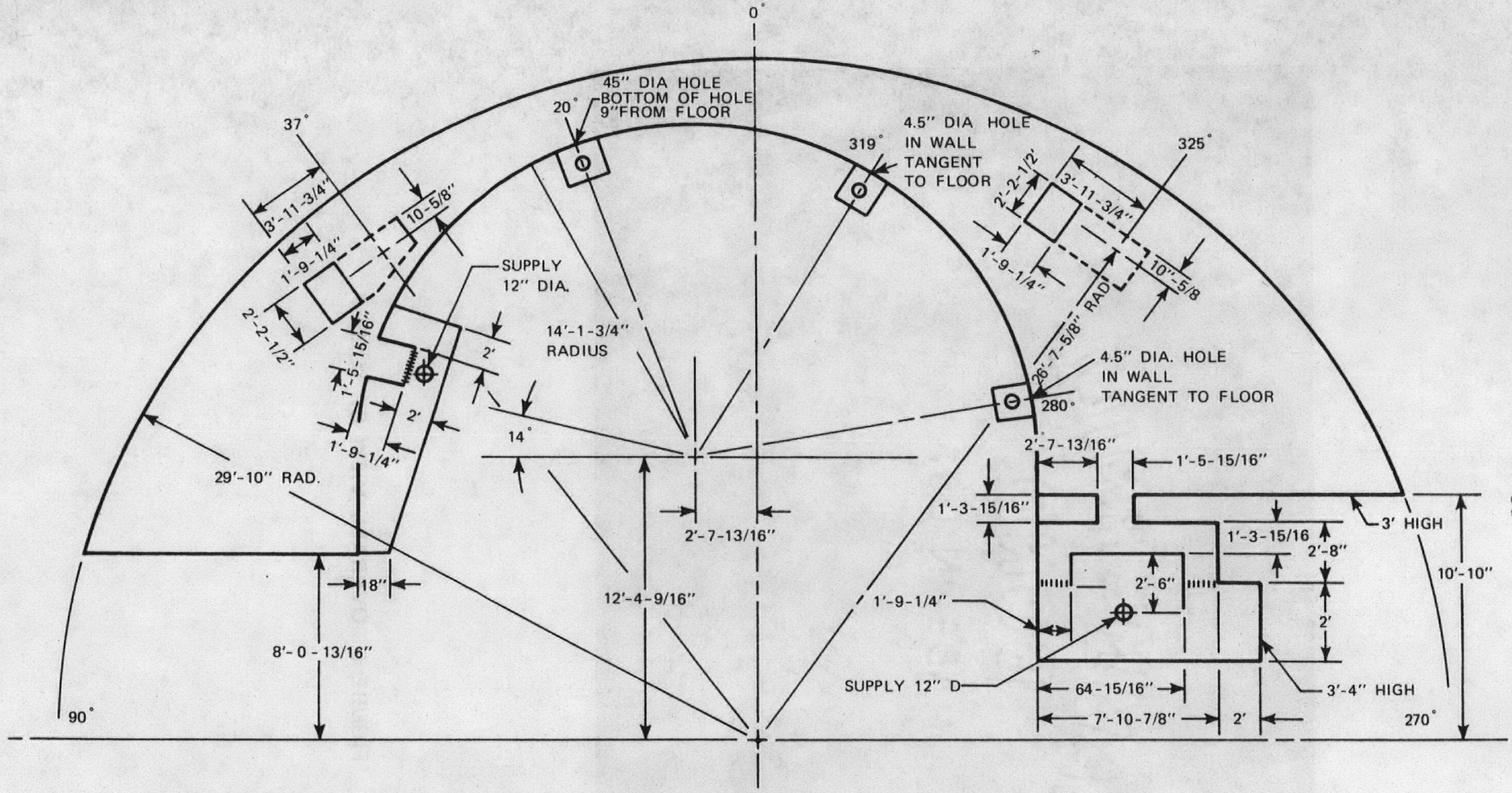

FIGURE 5 MODEL BOUNDRIES

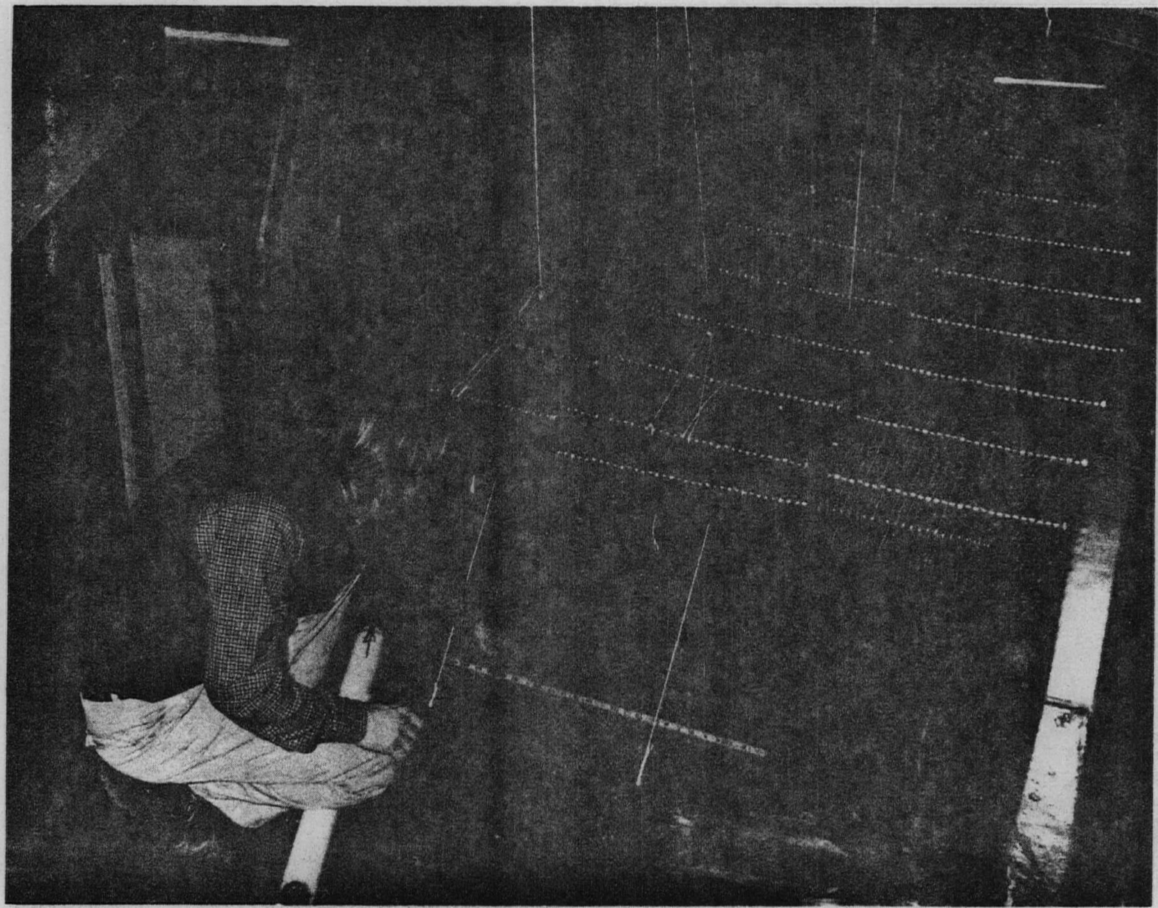

FIGURE 6 OVERALL VIEW OF SUMP A

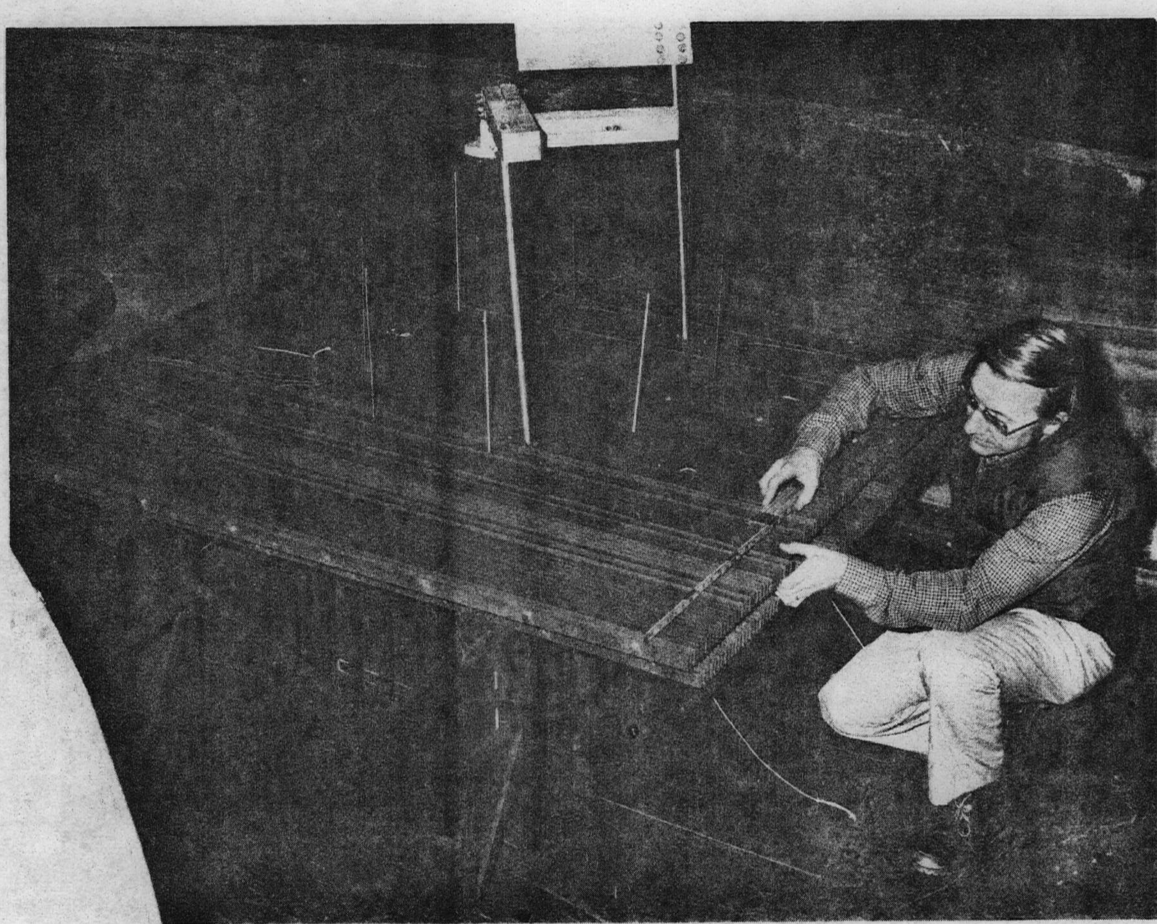

FIGURE 7 OVERALL VIEW OF SUMP B

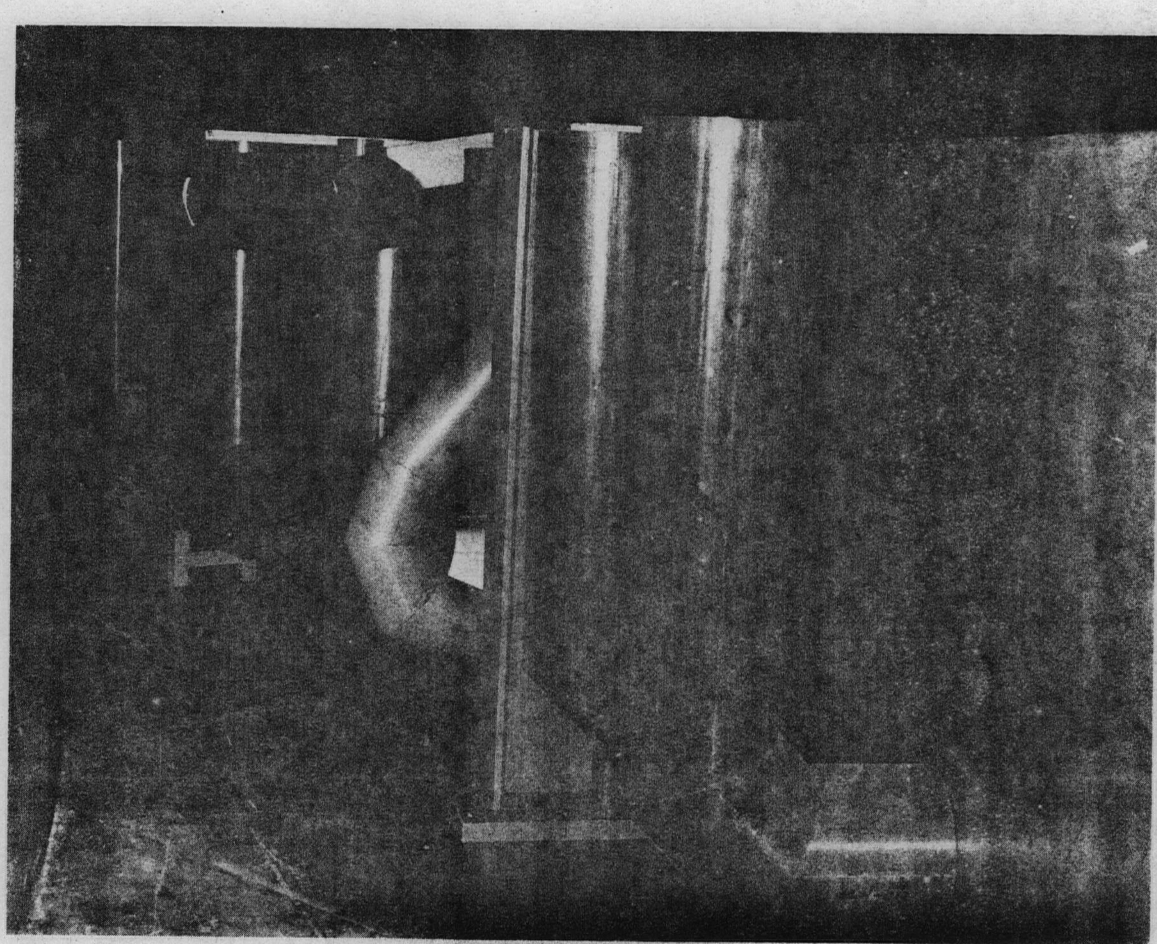

FIGURE 8 APPURTENANT STRUCTURES VIEWED FROM NEAR SUMP B TOWARDS SUMP A

VORTEX TYPE	
1	INCOHERENT SURFACE SWIRL
2	SURFACE DIMPLE; COHERENT SWIRL AT SURFACE
3	DYE CORE TO INTAKE; COHERENT SWIRL THROUGHOUT WATER COLUMN
4	VORTEX PULLING FLOATING TRASH, BUT NOT AIR
5	VORTEX PULLING AIR BUBBLES TO INTAKE
6	FULL AIR CORE TO INTAKE

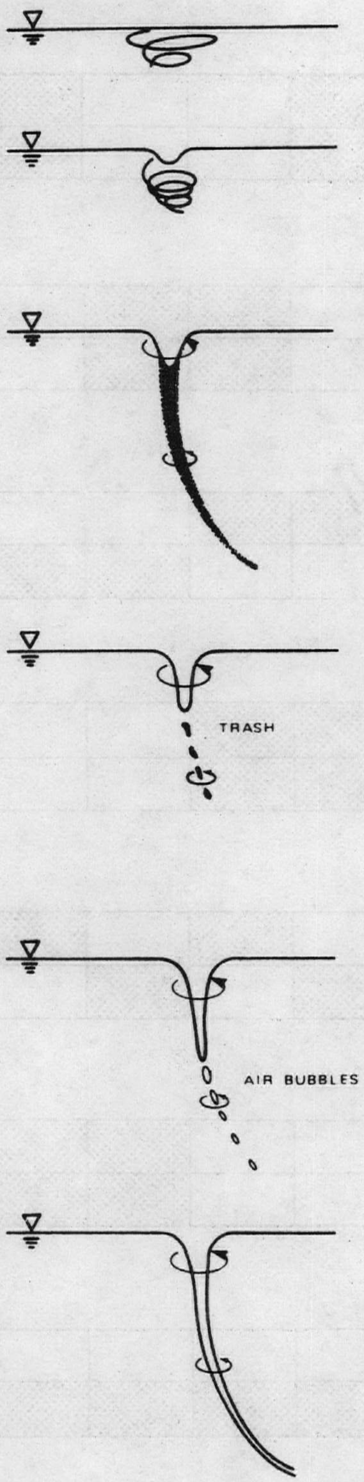

FIGURE 9 CLASSIFICATION OF FREE SURFACE VORTICES

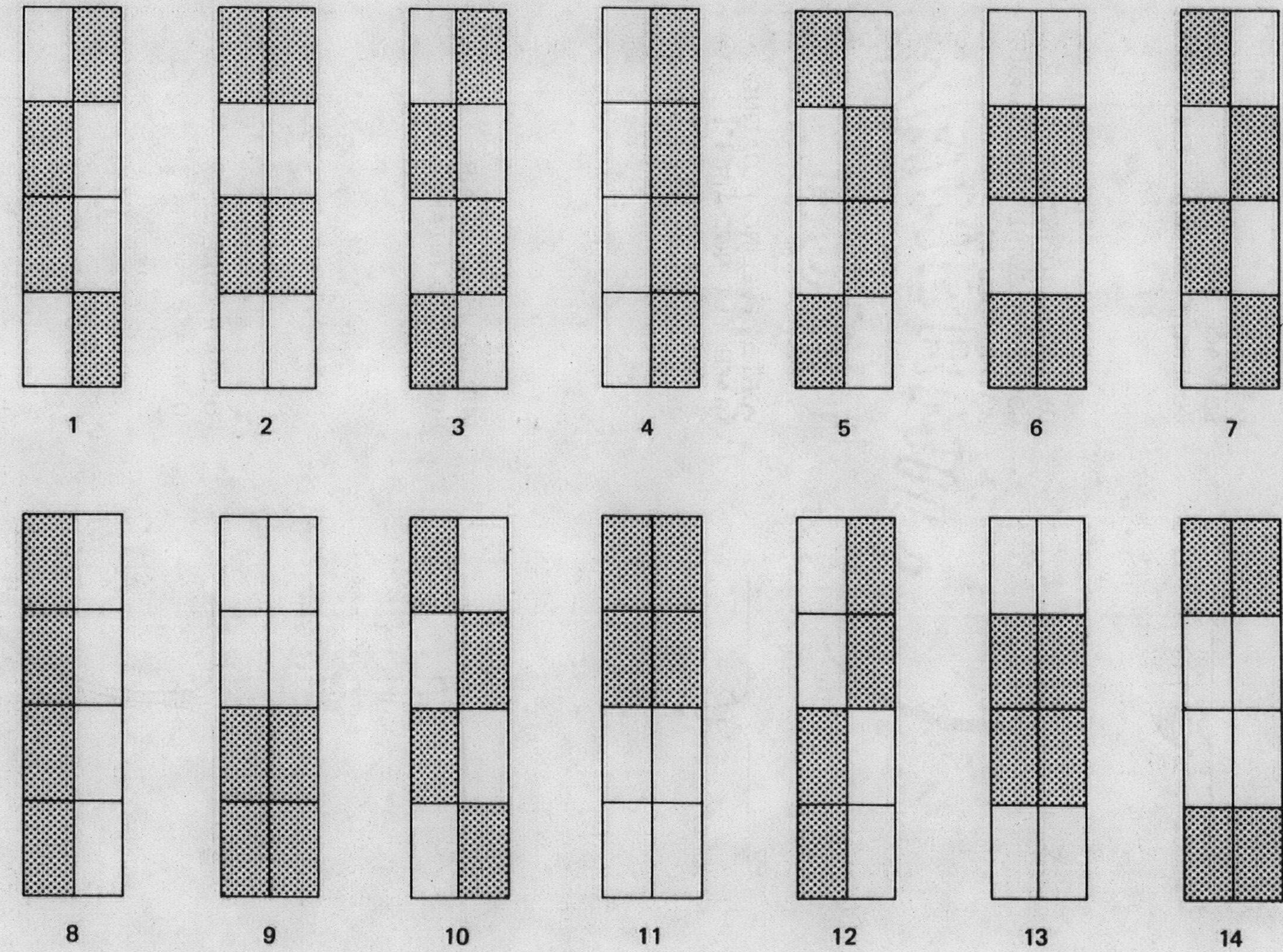

FIGURE 10 FINE SCREEN BLOCKAGES

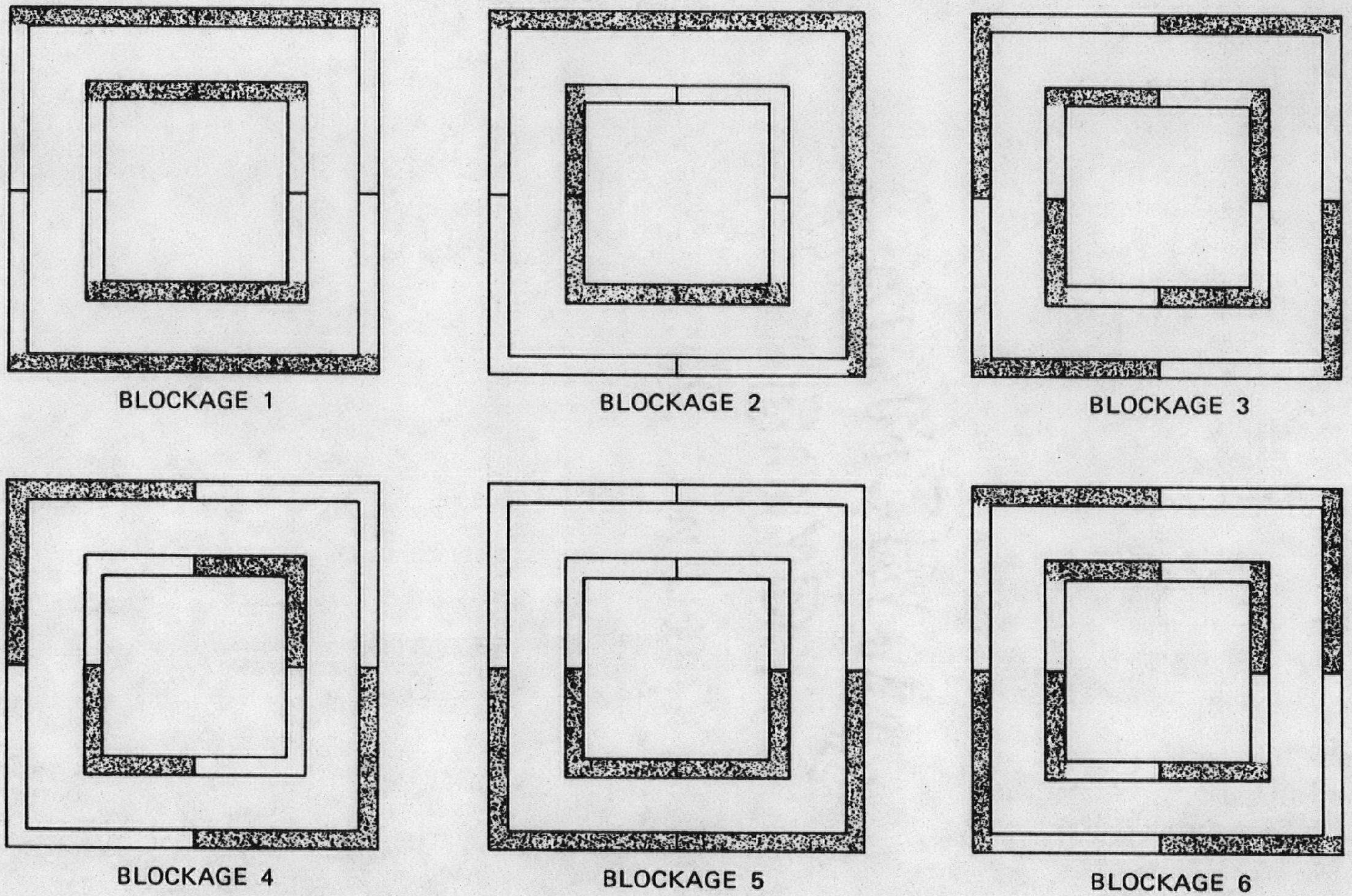

FIGURE 11 GRATING AND COARSE SCREEN BLOCKAGE SCHEMES